Nuclear Physics **A406** (1983) 369–389

CALCULATION OF THE IMAGINARY PART OF THE HEAVY ION POTENTIAL

G. POLLAROLO†, R. A. BROGLIA and A. WINTHER

The Niels Bohr Institute, University of Copenhagen, DK-2100 Copenhagen Ø, Denmark

Received 12 January 1983
(Revised 11 March 1983)

Abstract: The paper contains a numerical evaluation of the expressions for the absorptive potential in heavy ion reactions given earlier. With a standard folding expression for the real part of the ion-ion potential general good agreement is found with experimental data for the angular distributions of elastic and inelastic scattering. Special interest is attached to the case of $^{16}O + ^{28}Si$ where the calculated imaginary potential is very small at low bombarding energies.

1. Introduction

In the present paper we evaluate the imaginary part of the optical potential for a number of collisions between heavy ions. The calculations are made on the basis of the expressions derived in ref. [1]). The long-range part of this potential takes into account the depopulation of the entrance channel due to single-particle transfer. Multiparticle transfer as well as fusion are included to the extent that these processes go through successive steps of single-particle transfer.

Inelastic scattering due to processes where a particle goes back and forth between the two nuclei are thus also included. The major depopulation to inelastic channels take place, however, to collective states excited by the average field. This depopulation can be included as a separate contribution to the imaginary potential having a shorter range than the one due to particle transfer. The expression given in ref. [1]) for this potential is applicable only if the collective states are of vibrational type and are excited by the nuclear field only.

The calculation of the imaginary potential due to particle transfer and vibrations can be generalized to deformed nuclei by evaluating the associated quantities in the intrinsic system. They would then depend on the orientation of the system and have non-vanishing matrix elements connecting the rotational states. In this case Coulomb excitation often plays a dominant role. This excitation mechanism and its

† On leave from Istituto di Fisica Teorica dell'Università di Torino and INFN Sez. di Torino, Torino, Italy.

interference with nuclear inelastic scattering should be treated explicitly either classically or in the coupled-channel Born approximation.

In the present paper we calculate the imaginary potential for a number of reactions, where Coulomb excitation can be neglected. The results are applied to the analysis of elastic and inelastic differential cross sections at a variety of energies [2-5]). For the real part of the optical potential we have used the folded potential of ref. [6]).

In sect. 2 we give a resumé of the expression for the real and imaginary potentials. The calculation of $W(r)$ for the different reactions and energies as well as the comparison to the experimental data is presented in sect. 3. In sect. 4 the conclusions are presented.

2. Theoretical basis for the calculations

The basic assumption for the use of the imaginary potential as derived in ref. [1]) is that the depopulation of the elastic channel is due to a large number of independent transfer reactions and to nuclear inelastic scattering to a few collective vibrations. The imaginary potential can be written as

$$W(r) = W_{\text{trans}}(r) + W_{\text{inel}}(r). \tag{1}$$

The first component arises from the depopulation of the entrance channel due to single-particle transfer. It reads

$$W_{\text{trans}}(r) = \sum_{a,a',\lambda} \sqrt{\frac{a_{\text{tr}}(a_1, a_1')}{16\pi\hbar^2|\ddot{r}_0|}}$$

$$\times \{(2j_1'+1)U^2(a_1 I_A)V^2(a_1' I_a)|f_{\lambda 0}^{a_1' a_1(\text{NS})}(0,r)|^2$$

$$+ (2j_1+1)U^2(a_1' I_a)V^2(a_1 I_A)|f_{\lambda 0}^{a_1' a_1(\text{NP})}(0,r)|^2\} g_\lambda(Q). \tag{2}$$

The single-particle levels connected in the transition are labeled by $a_1 \equiv (n_1 l_1 j_1)$, n_1 indicating the number of nodes, while l_1 and j_1 are the orbital and total angular momenta. The quantity $a_{\text{tr}}(a_1 a_1')$ is the diffuseness of the form factor associated with the single-particle states a_1 and a_1', connected by the reaction. This quantity is, on average, of the order of 1.2 fm. The first term in (2) is connected with stripping reactions while the second term corresponds to pick-up.

The acceleration $\ddot{r}_0$ at the distance of closest approach for the grazing trajectory can be estimated through the expression

$$m_{aA}\ddot{r}_0 = (2E - E_B)/r_B, \tag{3}$$

valid for the Coulomb trajectory. The quantities E_B and r_B are the height and the radius of the Coulomb barrier [cf. ref. [7]), subsect. III.2], while E is the bombarding energy in the center-of-mass system.

The parameters U^2 and V^2 are the spectroscopic factors, thus,

$$V^2(a_1' I_a) = \frac{1}{2j_1'+1} \sum_{m_1'} |\langle I_a M_a | a^\dagger_{j_1' m_1'}(a_1') a_{j_1' m_1'}(a_1') | I_a M_a \rangle|^2 \tag{4}$$

is the probability that the single-particle orbital is occupied in nucleus a while the quantity $U^2 = 1 - V^2$ is the corresponding probability that the orbital a_1 is empty in the target A.

The function $g_\lambda(Q)$ which depends parametrically on the Q-value and on the angular momentum λ transferred in the reaction determines the adiabatic cut-off. That is, it weighs the probability with which the different transfer channels contribute to $W_{\text{trans}}(r)$.

The component of the imaginary potential arising from the nuclear inelastic scattering to vibrational states is

$$W_{\text{inel}}(r) = \left(\frac{a\pi}{\hbar^2 |\dot{r}_0|}\right)^{\frac{1}{2}} \sigma^2 \left(\frac{\partial U^N_{aA}}{\partial r}\right)^2, \tag{5}$$

where U^N_{aA} is the nuclear part of the ion-ion potential, while $a (\approx 0.6$ fm) is its diffuseness. In the quantity $\partial U/\partial r$ we recognize the collective form factor for inelastic excitations, while

$$\sigma^2 = \sum_\lambda \frac{2\lambda+1}{4\pi} \left(\frac{\hbar\omega^a_\lambda}{2C^a_\lambda} (R^{(0)}_a + \frac{\hbar\omega^A_\lambda}{2C^A_\lambda} (R^{(0)}_A)^2 \right) g_\lambda(\hbar\omega_\lambda) \tag{6}$$

is the square of the zero-point fluctuation of the surfaces of the two nuclei, weighed by the adiabatic cut-off.

The first term in (1) leads to a long-range component of the absorption with a diffuseness of the order of 0.6 fm. The second, to a short-range part with $a_W \approx 0.3$ fm.

The imaginary potential depends on the energy mainly through the function $g_\lambda(Q)$. As the bombarding energy increases, the collision time decreases leading to an increase of $g_\lambda(Q)$ and thus of W.

At higher bombarding energies ($E > 10$ MeV per nucleon) one should include the momentum dependence of the form factor as described in ref. [1]). The associated reduction of the contribution from each of the single-particle levels in part compensates for the increase due to the opening of the Q-window. These recoil effects are not included in the present paper.

3. Examples

In this section we present the results of the calculations for $W(r)$ associated with the scattering of ^{16}O on ^{208}Pb, ^{88}Sr, ^{40}Ca and ^{28}Si.

In fig. 1 we show the mass partitions which are populated in these collisions through single-particle transfer. The single-particle levels involved in the transfer processes can be read from the diagrams of fig. 2. They were calculated making use of the standard potential

$$V(r) = -V_0 f(a_0, r_0, r) + V_{\mathrm{Coul}}(r_{0c}, r)$$

$$+ V_{ls} r_{0s}^2 (\boldsymbol{l} \cdot \boldsymbol{s}) \frac{1}{r} \frac{\partial}{\partial r} f(a_{0s}, r_{0s}, r), \tag{7}$$

where

$$f(a, r_0, r) = (1 + \exp((r - R_0)/a))^{-1}, \tag{8}$$

$$R_0 = r_0 A^{\frac{1}{3}}. \tag{9}$$

The corresponding parameters are collected in table 1.

The resulting levels agree well with the observed experimental values for single-particle energies around the Fermi surface and for $A \gtrsim 100$. Deviation of the order of 0.5–1 MeV are observed for individual levels in lighter nuclei. In all the cases however, the correct sequence of levels is predicted.

The single-particle form factors for stripping reactions, defined as [cf. ref. [1]),

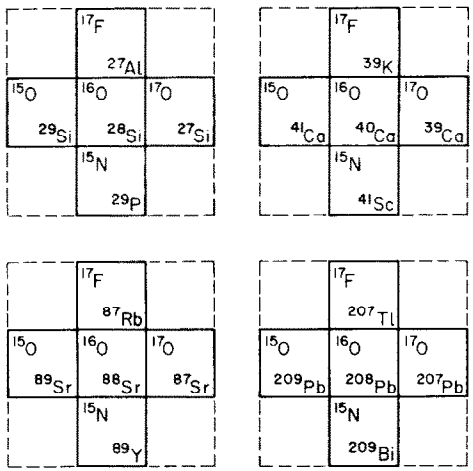

Fig. 1. Channels populated through single-particle transfer reactions from the collisions studied in this paper. The entrance channel partition is contained in the central block.

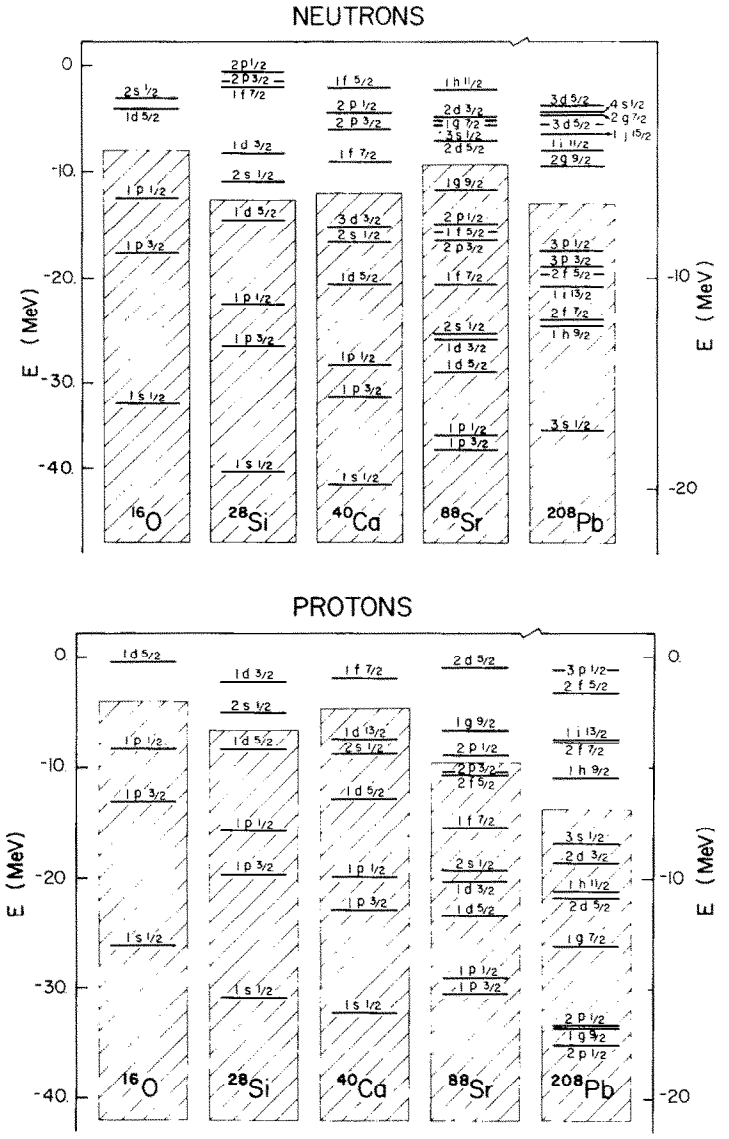

Fig. 2. Neutron and proton single-particle levels obtained from the single-particle potential (7) with the parameters of table 1. The hatched areas contain the levels below the Fermi surface. Note that the energy scale for ^{208}Pb is different from the others.

TABLE 1

The parameters for the shell-model potential (7) used to evaluate the form factors for the single-particle transfer reactions

		V_0	a_0	r_0	V_{ls}	r_{0s}	a_{0s}	r_{0c}
^{16}O	n	54.84	0.66	1.18	26.4	0.95	0.55	–
	p	55.16	0.66	1.18	26.4	0.95	0.55	1.10
^{28}Si	n	54.79	0.66	1.22	83.4	1.01	0.55	–
	p	55.21	0.66	1.22	83.4	1.01	0.55	1.11
^{40}Ca	n	54.75	0.66	1.23	22.1	1.04	0.55	–
	p	55.25	0.66	1.23	22.1	1.04	0.55	1.11
^{88}Sr	n	50.74	0.66	1.23	20.2	1.03	0.55	–
	p	59.26	0.66	1.24	20.2	1.03	0.55	1.11
^{208}Pb	n	47.76	0.66	1.24	18.8	1.13	0.55	–
	p	62.24	0.66	1.25	18.8	1.13	0.55	1.13

For each of the nuclei considered the parameters are given for neutrons (n) and protons (p) separately (in MeV and fm).

eq. (B.30) *et seq.*]

$$f^{a_1 a_1'}_{\lambda 0}(0,r) = 4\pi^{\frac{3}{2}}(2j_1+1)^{\frac{1}{2}}(-1)^{l_1'+\lambda+\frac{1}{2}}\begin{Bmatrix} l_1 & l_1' & \lambda \\ j_1' & j_1 & \frac{1}{2}\end{Bmatrix}\left(\frac{1}{2}\left(\frac{m_B}{m_A}+\frac{m_a}{m_b}\right)\right)^3$$
$$\times \int_{y>0} y\,dy\,dz R^{(A)}_{a_1}(r_{1A})(U_{1A}(r_{1A})-\langle U_{1A}\rangle)R^{(b)}_{a_1'}(r_{1b})$$
$$\sum_{m_1 m_1'} \langle l_1 m_1 l_1' m_1' | \lambda 0\rangle Y_{l_1 m_1}(\theta_A, 0) Y_{l_1' m_1'}(\theta_b, 0), \tag{10}$$

were calculated using for U_{1A} the potential (7) associated with the target nucleus and setting $V_{ls} = 0$. With the same potential the single-particle wave functions $R(r)$ were calculated. The quantity $\langle U_{1A}\rangle$ is written as

$$\langle U_{1A}\rangle = U^N_{aA}(r_{aA}) - U^N_{bA}(r_{bA}) + U^C_{aA}(r_{aA}) - U^C_{bA}(r_{bA}), \tag{11}$$

and was calculated making use of the Saxon-Woods parametrization to the ion-ion potential [cf. eq. (III.1.44) of ref. [7])], i.e.

$$U^N_{aA} = \frac{-V_0}{1+\exp((r-R_0)/a)}, \tag{12}$$

where

$$V_0 = 16\pi\gamma \frac{R_a R_A}{R_a + R_A} a,$$
$$a = 0.855[1+0.53(A_a^{-\frac{1}{3}} + A_A^{-\frac{1}{3}})]^{-1}\ \text{fm},$$
$$R_0 = R_a + R_A, \tag{13}$$

and

$$R_i = 1.20A_i^{\frac{1}{3}} - 0.09\,\text{fm}. \tag{14}$$

The quantity $\gamma = 1$ MeV $\cdot$ fm^{-2} is the surface tension parameter.

The form factors associated with pick-up processes appearing in (2) were calculated making use of a similar expression to (10) [cf. ref. [1])].

The resulting form factors were parametrized according to

$$f_{\lambda 0}(0, r) = F_0 e^{-(r-R)/a_{\text{tr}}}, \tag{15}$$

where the corresponding parameters are collected in table 2. In all cases spectroscopic factors equal to 1 have been assumed, i.e. $V^2(a_1' I_a) = U^2(a_1 I_A) = 1$ for stripping and $U^2(a_1' I_a) = V^2(a_1 I_A) = 1$ for pick-up reactions (cf. eq. (2)).

In order to calculate the absorptive potential associated with inelastic scattering we need the energy and the zero-point amplitudes of the different modes. The values for ^{16}O as well as for the different targets are given in table 3. To calculate the two components of the absorptive potential (2) and (5) one needs, aside from form factors, the adiabatic cut-off function $g_\lambda(Q)$. It depends parametrically on the Q-value of the reaction and on the transferred angular momentum through

$$a = a_0(Q - Q_{\text{opt}})$$

with

$$a_0 = (a_{\text{tr}}(a_1 a_1')/\hbar^2|\ddot{r}_0|)^{\frac{1}{2}}, \tag{16}$$

and

$$b = b_0\lambda,$$

with

$$b_0 = \left(\frac{a_{\text{tr}}(a_1 a_1')}{\hbar^2|\ddot{r}_0|}\right)\frac{\hbar^2(l_g + \frac{1}{2})}{m_{aA} r_0^2}. \tag{17}$$

The optimum Q-value is given by

$$Q_{\text{opt}} = \left(\frac{Z_d}{Z_A} - \frac{Z_d}{Z_b}\right)E_B + \left(\frac{m_d}{m_b} - \frac{m_d}{m_A}\right)(E - E_B)$$

$$+ \frac{m_d \ddot{r}_0}{m_a + m_A}(R_A m_b - R_a m_B), \tag{18}$$

where Z_d is the charge and m_d the mass of the transferred particle. The quantities are defined to be positive for stripping reactions and negative for pick-up reactions. They are zero for inelastic scattering. The height of the Coulomb barrier is denoted

TABLE 2

Form factors for single-particle transfer reactions considered in the evaluation of the absorptive potential

	$n_1'l_1'j_1'$	$n_1l_1j_1$	λ	F_0	a_{tr}	Q (MeV)
$^{15}O+^{209}Pb$	$1p_{1/2}$	$2g_{9/2}$	5	6.6	1.23	−7.68
		$1i_{11/2}$	5	1.0	1.22	−8.37
		$1j_{15/2}$	8	4.3	1.09	−9.25
		$3d_{5/2}$	3	4.8	1.45	−9.63
		$2g_{7/2}$	3	1.8	1.40	−10.15
		$4s_{1/2}$	1	2.2	1.62	−10.22
		$3d_{5/2}$	3	4.2	1.54	−10.52
	$1p_{3/2}$	$2g_{9/2}$	3	2.0	1.17	−12.81
			5	3.3	1.13	−12.81
		$1i_{11/2}$	5	0.5	1.10	−13.50
			7	3.3	1.05	−13.50
		$1j_{15/2}$	6	0.9	1.07	−14.38
			8	2.2	1.01	−14.38
		$3d_{5/2}$	1	1.8	1.39	−14.76
			3	2.4	1.36	−14.76
		$2g_{7/2}$	3	0.7	1.30	−15.28
			5	3.6	1.25	−15.28
		$4s_{1/2}$	1	1.7	1.54	−15.35
		$3d_{5/2}$	1	1.6	1.49	−15.65
			3	2.1	1.46	−15.65
$^{17}O+^{207}Pb$	$1d_{5/2}$	$3p_{1/2}$	3	5.2	1.37	−4.77
		$3p_{3/2}$	1	2.2	1.38	−5.52
			3	3.3	1.33	−5.52
		$2f_{5/2}$	1	0.2	1.35	−5.84
			3	0.8	1.31	−5.84
			5	5.2	1.23	−5.84
		$1i_{13/2}$	4	0.2	1.25	−6.47
			6	0.4	1.16	−6.47
			8	1.9	1.07	−6.47
		$2f_{7/2}$	1	0.8	1.24	−8.02
			3	1.2	1.21	−8.02
			5	2.8	1.15	−8.02
		$1h_{9/2}$	3	0.1	1.19	−8.33
			5	0.5	1.13	−8.33
			7	3.7	1.06	−8.33
	$2s_{1/2}$	$3p_{1/2}$	1	4.0	1.45	−5.65
		$3p_{3/2}$	1	4.0	1.41	−6.40
		$2f_{5/2}$	3	2.8	1.33	−6.72
		$1i_{13/2}$	6	1.1	1.17	−7.35
		$2f_{7/2}$	3	2.7	1.24	−8.90
		$1h_{9/2}$	5	1.4	1.15	−9.21
$^{15}N+^{209}Bi$	$1p_{1/2}$	$1h_{9/2}$	4	1.4	1.18	−2.84
		$2f_{7/2}$	4	7.6	1.17	−4.50
		$1i_{13/2}$	7	5.3	1.06	−4.51
		$2f_{5/2}$	2	2.9	1.18	−6.64
		$3p_{1/2}$	0	3.1	1.18	−7.69
	$1p_{3/2}$	$1h_{9/2}$	4	0.8	0.97	−7.83
			6	4.8	0.93	−7.83

TABLE 2 (continued)

	$n_1'l_1'j_1'$	$n_1l_1j_1$	λ	F_0	a_{tr}	Q (MeV)
	$1p_{3/2}$	$2f_{7/2}$	2	3.3	0.97	−9.49
			4	4.9	0.95	−9.49
		$1i_{13/2}$	5	1.5	0.93	−9.50
			7	3.4	0.89	−9.50
		$2f_{5/2}$	2	1.6	0.92	−11.63
			4	7.8	0.90	−11.63
		$3p_{1/2}$	2	7.4	0.85	−12.68
$^{17}F+^{207}Tl$	$1d_{5/2}$	$3s_{1/2}$	2	0.8	1.17	−8.07
		$2d_{3/2}$	2	0.3	1.05	−8.91
			4	0.6	1.23	−8.91
		$1h_{11/2}$	3	2.9	0.62	−10.15
			5	1.5	0.69	−10.15
			7	0.4	0.95	−10.15
		$2d_{5/2}$	0	0.3	1.06	−10.43
			2	0.3	1.16	−10.43
			4	0.2	1.36	−10.43
		$1g_{7/2}$	2	0.2	0.82	−12.64
			4	0.2	0.96	−12.64
			6	0.1	1.41	−12.64
$^{15}O+^{89}Sr$	$1p_{1/2}$	$2d_{5/2}$	3	7.7	1.20	−5.61
		$2s_{1/2}$	1	3.9	1.29	−7.04
		$1g_{7/2}$	3	1.7	1.21	−7.51
		$2d_{3/2}$	1	2.9	1.29	−7.63
		$1h_{11/2}$	6	5.8	1.10	−10.22
	$1p_{3/2}$	$2d_{5/2}$	1	3.1	1.10	−10.74
			3	4.4	1.06	−10.74
		$3s_{1/2}$	1	3.5	1.15	−12.17
		$1g_{7/2}$	3	0.8	1.07	−12.64
			5	4.5	1.02	−12.64
		$2d_{3/2}$	1	0.9	1.14	−12.76
			3	4.7	1.11	−12.76
		$1h_{11/2}$	4	1.4	1.07	−15.35
			6	3.1	1.01	−15.35
$^{17}O+^{87}Sr$	$1d_{5/2}$	$1g_{9/2}$	2	0.4	1.24	−7.66
			4	0.8	1.16	−7.66
			6	2.9	1.06	−7.66
	$2s_{1/2}$		4	1.9	1.17	−8.55
	$1d_{5/2}$	$2p_{1/2}$	3	6.3	1.09	−10.78
	$2s_{1/2}$		1	3.9	1.18	−11.66
	$1d_{5/2}$	$1f_{5/2}$	1	0.2	1.10	−11.59
			3	0.8	1.07	−11.59
			5	5.0	1.01	−11.59
	$2s_{1/2}$		3	2.2	1.10	−12.47
	$1d_{5/2}$	$2p_{3/2}$	1	2.7	1.09	−12.26
			3	3.9	1.06	−12.26
	$2s_{1/2}$		1	3.8	1.14	−13.15
	$1d_{5/2}$	$1f_{7/2}$	1	0.8	0.98	−16.56
			3	1.2	0.96	−16.56
			5	2.5	0.92	−16.56
	$2s_{1/2}$		3	2.1	1.00	−17.44

TABLE 2 (continued)

	$n_1'l_1'j_1'$	$n_1l_1j_1$	λ	F_0	a_{tr}	Q (MeV)
$^{15}N+^{89}Y$	$1p_{1/2}$	$2p_{1/2}$	0	3.1	1.28	0.69
		$1g_{9/2}$	5	6.8	1.11	−1.61
		$2d_{5/2}$	3	9.0	1.11	−7.26
	$1p_{3/2}$	$2p_{1/2}$	2	4.6	0.90	−8.30
		$1g_{9/2}$	3	2.4	0.87	−10.60
			5	4.3	0.84	−10.60
		$2d_{5/2}$	1	44.0	0.54	−16.25
			3	34.7	0.58	−16.25
$^{17}F+^{87}Rb$	$1d_{5/2}$	$2p_{3/2}$	1	11.8	0.68	−10.03
			3	21.5	0.64	−10.03
		$1f_{5/2}$	1	0.3	0.88	−10.04
			3	1.6	0.80	−10.04
			5	18.7	0.65	−10.04
		$1f_{7/2}$	1	4.4	0.62	−15.08
			3	3.7	0.66	−15.08
			5	3.8	0.69	−15.08
		$2s_{1/2}$	2	1.3	0.96	−18.96
		$1d_{3/2}$	2	0.2	0.95	−19.95
			4	0.5	1.05	−19.95
$^{15}O+^{41}Ca$	$1p_{1/2}$	$1f_{7/2}$	4	8.1	1.10	−3.30
		$2p_{3/2}$	2	7.2	1.21	−6.47
		$2p_{1/2}$	0	2.9	1.28	−8.00
		$1f_{5/2}$	2	1.9	1.26	−10.36
	$1p_{3/2}$	$1f_{7/2}$	2	2.6	1.02	−8.43
			4	4.6	0.97	−8.43
		$2p_{3/2}$	0	1.5	1.12	−11.60
			2	2.2	1.09	−11.60
		$2p_{1/2}$	2	4.0	1.11	−13.13
		$1f_{5/2}$	2	0.7	1.14	−15.49
			4	4.3	1.08	−15.49
$^{17}O+^{39}Ca$	$1d_{5/2}$	$1d_{3/2}$	2	1.0	1.10	−11.20
			4	6.3	1.04	−11.20
	$2s_{1/2}$		2	3.0	1.15	−12.08
	$1d_{5/2}$	$2s_{1/2}$	2	6.4	1.07	−12.65
	$2s_{1/2}$		0	4.5	1.16	−13.53
	$1d_{5/2}$	$1d_{5/2}$	0	1.1	1.00	−16.68
			2	1.7	0.98	−16.68
			4	3.3	0.95	−16.68
	$2s_{1/2}$		2	2.6	1.05	−17.56
$^{15}N+^{41}Sc$	$1p_{1/2}$	$1f_{7/2}$	4	7.9	1.09	−6.47
	$1p_{3/2}$		2	3.4	0.90	−11.46
			4	6.2	0.87	−11.46
$^{17}F+^{39}K$	$1d_{5/2}$	$1d_{3/2}$	2	1.1	1.07	−6.91
			4	7.4	1.01	−6.91
		$2s_{1/2}$	2	8.1	1.00	−8.24
		$1d_{5/2}$	0	2.8	0.77	−12.32
			2	3.4	0.79	−12.32
			4	6.3	0.78	−12.32

TABLE 2 (continued)

	$n_1'l_1'j_1'$	$n_1l_1j_1$	λ	F_0	a_{tr}	Q (MeV)
$^{15}O+^{29}Si$	$1p_{1/2}$	$2s_{1/2}$	1	5.9	1.18	−1.59
		$1d_{3/2}$	1	2.9	1.19	−4.33
		$1f_{7/2}$	4	7.1	1.16	−10.65
		$2p_{3/2}$	2	4.9	1.36	−11.11
		$2p_{1/2}$	0	1.5	1.59	−12.06
	$1p_{3/2}$	$2s_{1/2}$	1	5.4	1.02	−6.72
		$1d_{3/2}$	1	0.9	1.03	−9.46
			3	5.4	1.00	−9.46
		$1f_{7/2}$	2	2.1	1.11	−15.78
			4	3.8	1.06	−15.78
		$2p_{3/2}$	0	1.9	1.30	−16.24
			2	1.1	1.37	−16.24
		$2p_{1/2}$	2	1.8	1.48	−17.19
$^{17}O+^{27}Si$	$1d_{5/2}$	$1d_{5/2}$	0	1.1	1.15	−10.38
			2	1.8	1.12	−10.38
			4	4.2	1.06	−10.38
	$2s_{1/2}$		2	3.4	1.16	−11.27
	$1d_{5/2}$	$1p_{1/2}$	3	5.0	0.96	−18.40
	$2s_{1/2}$		1	2.5	1.08	−19.29
$^{15}N+^{29}P$	$1p_{1/2}$	$2s_{1/2}$	1	5.4	1.24	−3.29
		$1d_{3/2}$	1	2.7	1.18	−5.94
	$1p_{3/2}$	$2s_{1/2}$	1	6.0	0.98	−8.28
		$1d_{3/2}$	1	1.6	0.86	−10.92
			3	9.2	0.85	−10.92
$^{17}F+^{27}Al$	$1d_{5/2}$	$1d_{5/2}$	0	1.2	1.08	−7.97
			2	2.1	1.04	−7.97
			4	5.5	0.99	−7.97
		$1p_{3/2}$	3	5.6	0.87	−15.40

For each channel the quantum numbers for the state in the projectile and in the target are given in columns 2 and 3, respectively, while column 4 indicates the total angular momentum transfer λ. Columns 5 and 6 contain the strength (in MeV) and the decay length (in fm) of the corresponding form factor (cf. eq. (15)) with $R = 1.20\ (A_a^{1/3}+A_A^{1/3})$ fm. They were calculated from wave functions in the standard shell model (7) with the parameters given in table 1. The last column is the Q-value for the single-particle transfer in this shell model.

by E_B. The quantity l_g is the grazing angular momentum, while m_{aA} denotes the reduced mass and r_0 the distance of closest approach [cf. eqs. (III.3.28) and (III.2.6), ref. [7])].

In table 4 are given the coefficients a_0, b_0 for $a_{tr} = 1$ fm and Q_{opt} for the different reactions analyzed below. An illustration of the function $g_\lambda(Q)$ is shown in fig. 3.

$^{16}O+^{208}Pb$. In the calculation of the absorptive potential for the scattering of ^{16}O on ^{208}Pb we have included the single-particle transfer processes given in table 2. We have also included the inelastic transitions to the levels of ^{16}O and of ^{208}Pb shown in table 3.

TABLE 3

The collective states included in the evaluation of the imaginary potential due to inelastic scattering

	λ	E_x	$B_{s.p.u.}(E\lambda)$	$\|\beta\|$
^{208}Pb	2^+	4.10	10.8	0.061
	3^-	2.6	32.0	0.12
	4^+	4.3	15.0	0.07
	5^-	3.3	17.0	0.067
^{88}Sr	2^+	1.84	4.5	0.12
	3^-	2.73	13.6	0.206
^{40}Ca	2^+	3.9	2.0	0.112
	3^-	3.7	12.0	0.27
	4^+	7.9	2.8	0.127
	5^-	4.5	9.0	0.22
^{28}Si	2^+	1.78	12.6	0.38
	3^-	6.88	25.0	0.56
^{16}O	2^+	6.92	3.4	0.36
	3^-	6.13	5.6	0.46

For each state of spin λ, the excitation energy (in MeV), the $B(E\lambda)$ value in single-particle units and the deformation parameter is given.

From the Q-values and excitation energies one evaluates the function $g_\lambda(Q)$. The results associated with the transfer reaction for four bombarding energies are shown in fig. 3. Each transition is indicated by a point. The figure illustrates how at the higher bombarding energies more transitions contribute.

The resulting imaginary potential $(W(r))_{\text{trans}}$ can be fitted by

$$W_{\text{trans}}(r) = \frac{W_0(E)}{1+\exp\left((r-R_0)/a_W\right)}, \tag{19}$$

with R_0 given by (13) since the internal part of the potential is irrelevant. The resulting parameters $W_0(E)$ and a_W are given in table 5.

The imaginary part of the potential arising from inelastic processes is given by

$$W_{\text{inel}}(r) = K(E)\left(\frac{\partial U^{\text{N}}_{\text{aA}}(r)}{\partial r}\right)^2. \tag{20}$$

The values of K for the different bombarding energies are also collected in table 5. The real part of the ion-ion potential $U_{\text{aA}}(r)$ is given in eq. (12).

With these ingredients the differential cross sections for elastic scattering were evaluated with the optical model code GENOA [9]). The results are compared to the experimental data in fig. 4. While the agreement is good at higher bombarding energies, one notices an important discrepancy at the lower bombarding energies.

TABLE 4

Parameters for the determination of the adiabatic cut-off

	E_{lab}	Q_{opt} (MeV)				a_0	b_0
	(MeV)	n.s.	n.p.	p.s.	p.p	$(MeV)^{-1}$	
$^{16}O+^{206}Pb$	88	0.78	+0.78	−10.70	8.30	0.213	0.152
	96	−0.52	0.57	−10.45	8.10	0.203	0.211
	102	−0.32	0.40	−10.25	7.93	0.193	0.238
	104	−0.25	0.35	−10.18	7.87	0.190	0.245
	129.5	0.60	−0.34	− 9.35	7.18	0.160	0.299
	138.5	0.90	−0.58	− 9.03	6.94	0.152	0.309
	192	2.68	−2.02	− 7.25	5.50	0.122	0.340
$^{16}O+^{88}Sr$	48	−0.51	0.46	− 5.21	3.88	0.285	0.062
	52	−0.40	0.38	− 5.11	3.80	0.264	0.198
	56	−0.30	0.30	− 5.00	3.72	0.247	0.254
	59	−0.23	0.23	− 4.93	3.66	0.236	0.282
$^{16}O+^{40}Ca$	40	−0.14	0.10	− 2.33	1.54	0.273	0.319
	50	0.01	−0.29	− 2.18	1.41	0.229	0.407
	74	0.37	−0.34	− 1.82	1.11	0.174	0.466
	104	0.82	−0.72	− 1.38	0.72	0.141	0.484
	140	1.56	−1.18	− 0.83	0.26	0.119	0.488
$^{16}O+^{28}Si$	36	−0.06	0.01	− 1.29	0.69	0.273	0.393
	55	0.12	−0.15	− 1.11	0.53	0.200	0.480
	81	0.36	−0.38	− 0.87	0.31	0.157	0.515
	141	0.91	−0.89	− 0.32	−0.20	0.114	0.519

For each reaction and at each bombarding energy are given the optimum Q-values for neutron stripping (n.s.) and pick-up (n.p.) and for proton stripping (p.s.) and pick-up (p.p.). The quantities a_0 and b_0 (cf. eqs. (16) and (17)) are given in the last two columns for the case of $a_{tr} = 1$ fm.

We have also calculated differential cross sections for inelastic scattering for the 2^+, 3^- and 5^- states in ^{208}Pb at a bombarding energy of 104 MeV. The results are given in fig. 5 together with the experimental data.

For the highest bombarding energy of 192 MeV some states not included in the single-particle spectrum might contribute leading to an underestimate of the potential. On the other hand, at this bombarding energy one should include recoil effects which would diminish the form factors and thus the absorption.

$^{16}O+^{88}Sr$. With the single-particle form factors of table 2 and the inelastic channels given in table 3 we obtain the parameters for the imaginary potential given in table 6. The resulting elastic scattering angular distributions are compared with the experimental data in fig. 6.

$^{16}O+^{40}Ca$. Similar calculations for the scattering of ^{16}O+^{40}Ca leads to the imaginary potential given in table 7. The associated elastic angular distributions are given in fig. 7.

$^{16}O+^{28}Si$. The imaginary potential for the scattering of ^{16}O+^{28}Si as calculated with the single-particle transitions shown in table 2 is given in table 8. Elastic

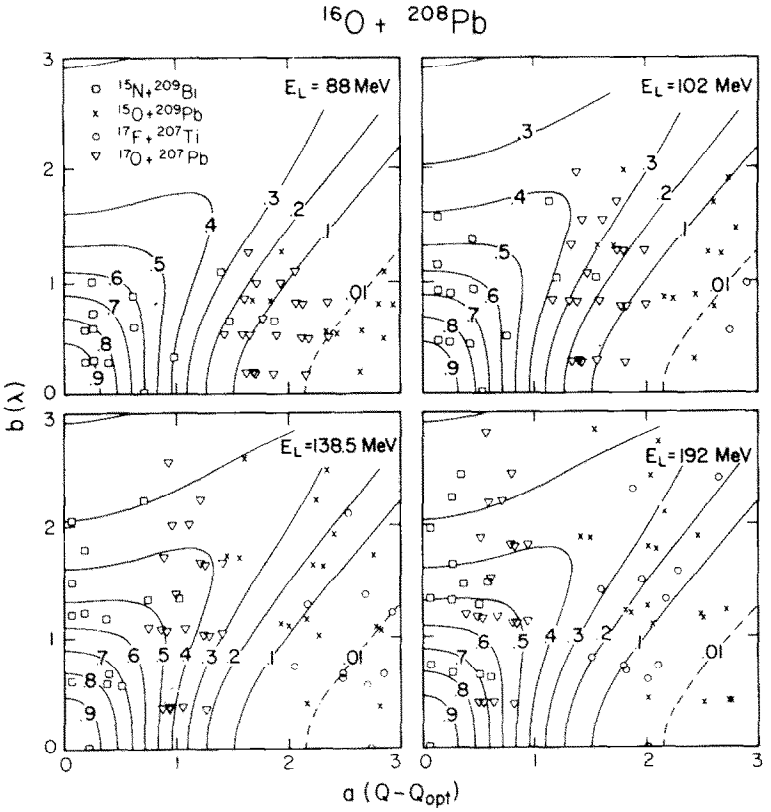

Fig. 3. The adiabatic cut-off function $g_\lambda(Q)$ for the reaction $^{16}O+^{208}Pb$. To display the energy dependence of the W_{trans} we have shown how the different single-particle transfer channels move in the (a, b) plane defining the adiabatic cut-off. The values of the function $g_\lambda(Q)$ are represented by contour lines. The different channels given in table 2 are represented by dots according to the legend in the left upper corner.

TABLE 5

The absorptive potential for the scattering of ^{16}O on ^{208}Pb (the parameters of eqs. (19) and (20) are given at various bombarding energies)

E_L	$E_{c.m.}/E_B$	$W_0(E)$ (MeV)	a_W (fm)	$K(E)$ (fm$^2\cdot$MeV^{-1})
88	1.07	−27.40	0.54	−0.043
96	1.17	−28.16	0.56	−0.045
102	1.25	−28.04	0.57	−0.046
104	1.27	−27.90	0.58	−0.046
129.5	1.58	−24.68	0.60	−0.046
138.5	1.69	−23.60	0.60	−0.045
192	2.34	−10.10	0.61	−0.042

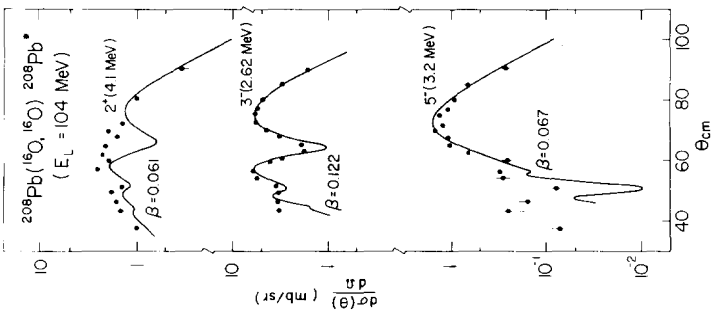

Fig. 5. Differential cross section for the inelastic scattering of ^{16}O on ^{208}Pb at a bombarding energy of 104 MeV. The full line indicates the results of a DWBA calculation with the optical potential of fig. 4 and the deformation parameters indicated. The dots represent the experimental points of ref. [2]).

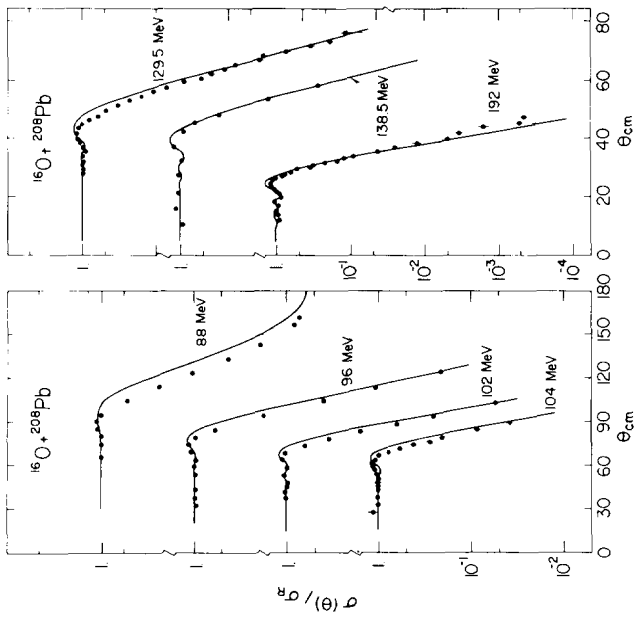

Fig. 4. The ratio of elastic to Rutherford angular distribution for the $^{16}O + ^{208}Pb$ reaction at different bombarding energies. The curves are calculated with the real potential (12) and with the imaginary potential of table 5. The data points are from ref. [2]).

TABLE 6

The absorptive potential for the scattering of ^{16}O on ^{88}Sr (the parameters of eqs. (19) and (20) are given at various bombarding energies)

E_L	$E_{c.m.}/E_B$	$W_0(E)$ (MeV)	a_W (fm)	$K(E)$ (fm^2 · MeV^{-1})
48	1.01	−21.30	0.53	−0.026
52	1.09	−23.37	0.53	−0.031
56	1.17	−28.80	0.52	−0.034
59	1.24	−34.70	0.52	−0.036

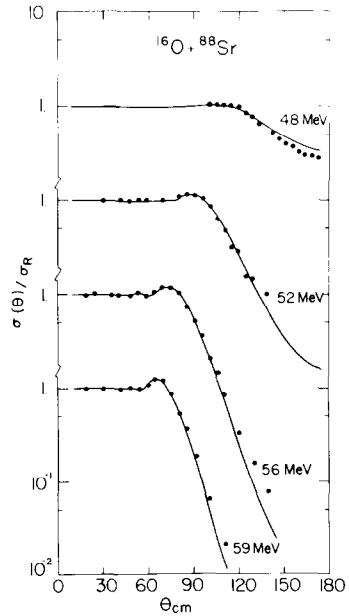

Fig. 6. The ratio of elastic to Rutherford angular distribution for the $^{16}O+^{88}Sr$ reaction at different bombarding energies. The curves are calculated with the real potential (12) and with the imaginary potential of table 6. The data points are from ref. [3]).

TABLE 7

The absorptive potential for the scattering of ^{16}O on ^{40}Ca (the parameters of eqs. (19) and (20) are given at various bombarding energies)

E_L	$E_{c.m.}/E_B$	$W_0(E)$ (MeV)	a_W (fm)	$K(E)$ (fm^2 · MeV^{-1})
40	1.21	− 9.54	0.54	−0.055
50	1.51	−13.67	0.53	−0.059
74	2.24	−17.23	0.52	−0.055
104	3.14	−17.11	0.52	−0.050
140	4.23	−15.92	0.52	−0.045

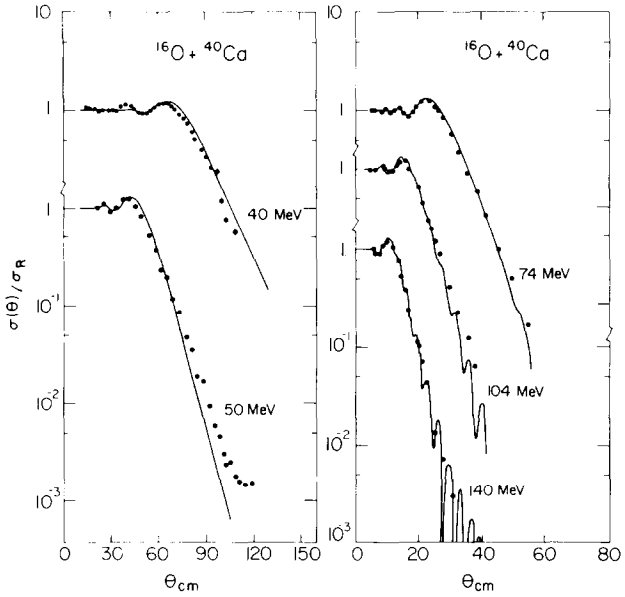

Fig. 7. The ratio of elastic to Rutherford angular distribution for the $^{16}O + ^{40}Ca$ reaction at different bombarding energies. The curves are calculated with the real potential (12) and with the imaginary potential of table 7. The data points are from ref. [4]).

scattering angular distributions are compared with the data in fig. 8. The theoretical prediction miss the backward rise shown by the data at the lowest bombarding energies.

For these bombarding energies the absorptive potential is, however, very sensitive to the Q-value of the single-particle transfer reactions. The results above are based on Q-values calculated with the average single-particle potential (7). We have recalculated W taking into account the experimental single-particle spectrum for both target and projectile (cf. fig. 9). The resulting potential for different bombarding energies is shown in fig. 10 and table 9. One observes that $W_{trans}(r)$

TABLE 8

The absorptive potential for the scattering of ^{16}O on ^{28}Si (the parameters of eqs. (19) and (20) are given at various bombarding energies)

E_L	$E_{c.m.}/E_B$	$W_0(E)$ (MeV)	a_W (fm)	$K(E)$ (fm$^2 \cdot$ MeV^{-1})
36	1.33	− 9.65	0.57	−0.098
55	2.03	−17.16	0.54	−0.100
81	3.00	−17.55	0.54	−0.085
141	5.25	−14.98	0.55	−0.065

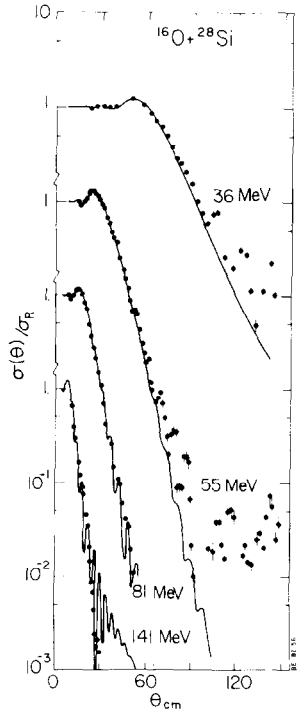

Fig. 8. The ratio of elastic to Rutherford angular distribution for the $^{16}O+^{28}Si$ reaction at different bombarding energies. The curves are calculated with the real potential (13) and with the imaginary potential of table 8. The data points are from ref. [5]).

depends strongly on the energy and becomes very small at bombarding energies close to the Coulomb barrier. In fig. 10 we have indicated by a dotted curve the potential W_{inel} at 33 MeV. As is seen from fig. 11 the absorption is dominated by inelastic scattering almost exclusively to the lowest 2^+ state in ^{28}Si (cf. table 3).

TABLE 9

The absorptive potential due to single-particle transfer for the scattering of ^{16}O on ^{28}Si (the parameters of eq. (19) were calculated on the basis of the experimental single-particle energies, cf. fig. 9)

	E_L (MeV)	$W_0(E)$ (MeV)	R_0 (fm)	a_W (fm)
$^{16}O+^{28}Si$	33	−0.50	6.00	0.55
	36	−1.60	6.00	0.525
	55	−5.0	6.50	0.50
	81	−6.0	6.50	0.53
	141	−7.5	6.50	0.53

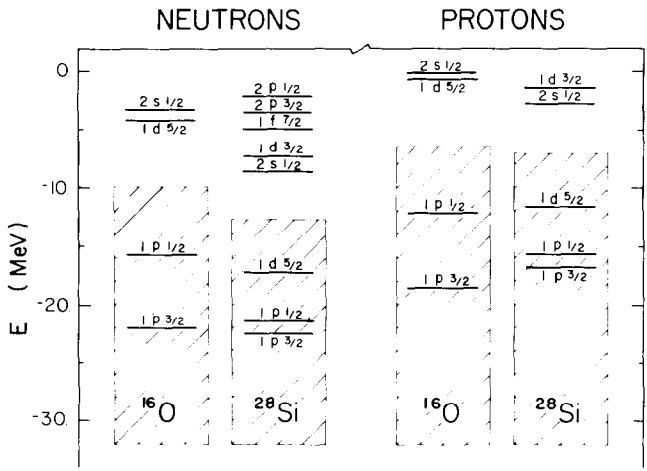

Fig. 9. The "experimental" single-particle spectrum for the single-particle motion of neutrons and protons in ^{16}O and ^{28}Si. (cf. fig. 2).

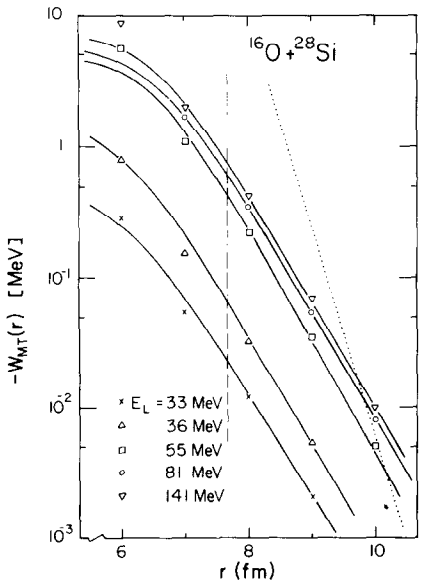

Fig. 10. The absorptive potential W_{trans} as calculated from the single-particle spectrum of fig. 9 for different bombarding energies. The full drawn curves indicate the Saxon-Woods fit to the calculations, the parameters of which are given in table 9. The dotted curve indicates the absorptive potential at 33 MeV due to inelastic scattering treating the 2^+ state of ^{28}Si as a vibrational state.

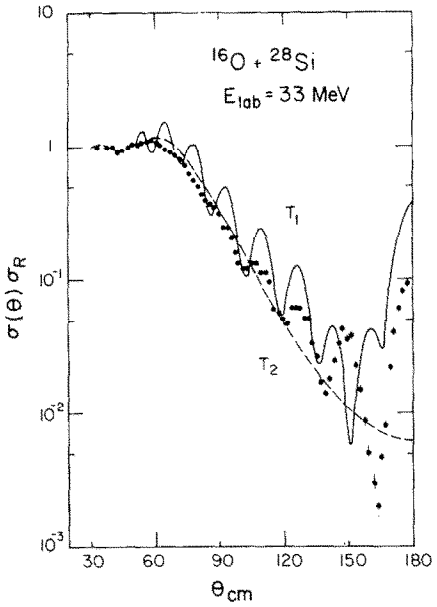

Fig. 11. The ratio of elastic to Rutherford angular distribution for $^{16}O + ^{28}Si$ at 33 MeV bombarding energy. The data points are from ref. [5]). The full drawn curve (T_1) is obtained in an optical model calculation where the real potential is given by (13) while the imaginary potential is given by $W_{trans}(r)$ of fig. 10. The dashed curve (T_2) is obtained by treating the collective state in ^{28}Si as a harmonic vibration.

This is however not a vibrational state was as assumed. It is well established that ^{28}Si is deformed, and as was mentioned earlier [cf. also ref. [1])] the inelastic scattering must in this case be treated by coupled channels with deformed potentials. Such calculations which are in progress show that the angular distributions are then much in agreement with the experimental results [10]).

4. Conclusions

Although some discrepancies remain, the overall agreement between the data and the theoretical calculations, based solely on nuclear structure information, gives us confidence that a detailed understanding of the grazing collisions can be obtained. The calculation of $W(r)$ should be improved to incorporate besides the experimental single-particle energies also the spectroscopic factors as obtained from the measured single-particle transfer cross sections. Since the latter not only enters through a multiplicative factor but also through the derived absorptive potential, this improvement must be done self-consistently.

References

1) R. A. Broglia, G. Pollarolo and A. Winther, Nucl. Phys. **A361** (1981) 307
2) F. Videbæk, R. B. Goldstein, L. Grodzins, S. A. Steadman, T. A. Belote and J. D. Garrett, Phys. Rev. **C15** (1977) 954;
F. Becchetti, D. G. Kovar, B. G. Harvey, J. Mahoney, B. Mayer and F. G. Pühlhofer, Phys. Rev. **C6** (1972) 2215;
J. B. Ball, C. B. Fulmer, E. E. Gross, M. L. Halbert, D. C. Hensley, C. A. Ludermann, M. J. Saltmarsh and G. R. Satchler, Nucl. Phys. **A252** (1975) 208;
S. C. Pieper, M. H. Macfarlane, D. H. Gloeckner, D. G. Kovar, F. D. Becchetti, B. G. Harvey, D. L. Hendrie, H. Homeyer, J. Mahoney, F. Pühlhofer, W. von Oertzen and M. S. Zisman, Phys. Rev. **C18** (1978) 180
3) D. Arantaraman, Phys. Rev. **C8** (1973) 2245;
F. Videbæk, private communication
4) K. O. Groeneveld, L. Meyer-Schützmeister, A. Richter and U. Strohbusch, Phys. Rev. **C6** (1972) 805;
S. Kubono, P. D. Bond and C. E. Thorn, Preprint BNL-24804;
S. E. Vigdor *et al.*, Phys. Rev. **C20** (1979) 2147
5) J. G. Cramer, R. H. deVries, D. A. Goldberg, M. S. Zisman and C. F. Maguire, Phys. Rev. **C14** (1976) 2158;
P. Braun-Munzinger, G. M. Berkowitz, M. Gai, C. M. Jochanski, T. R. Renner, C. D. Uhlhorn, J. Barrette and M. J. LeVine, Phys. Rev. **C24** (1981) 1010, and references therein;
P. Braun-Munzinger and J. Barrette, Phys. Reports **87** (1982) 209
6) Ö. Akyuz and A. Winther, in Proc. Enrico Fermi Int. School of Physics, 1979, course on nuclear structure and heavy ion reactions, ed. R. A. Broglia, C. H. Dasso and R. Ricci (North-Holland, Amsterdam, 1981)
7) R. A. Broglia and A. Winther, Heavy ion reactions (Benjamin/Cummings, Reading, Mass., 1981)
8) W. D. Myers, Nucl. Phys. **A145** (1970) 387; **A204** (1973) 465
9) F. G. Perey, unpublished
10) G. Pollarolo, S. Kahana, A. Winther, J. Barrette and R. A. Broglia, in preparation